

Amortized Phylodynamic Inference with Neural Bayes Estimators and Recursive Neural Networks

Alexander E. Zarebski *¹, Thomas Williams ,^{2,3} and Louis du Plessis ^{4,5}

¹MRC Biostatistics Unit, University of Cambridge, United Kingdom

²ARC Centre of Excellence for the Mathematical Analysis of Cellular Systems, The University of Melbourne, Australia

³School of Mathematics and Statistics, The University of Melbourne, Australia

⁴Department of Biosystems Science and Engineering, ETH Zürich, Switzerland

⁵Swiss Institute of Bioinformatics (SIB), Switzerland

Abstract

Phylodynamics is used to estimate epidemic dynamics from phylogenetic trees or genomic sequences of pathogens, but the likelihood calculations needed can be challenging for complex models. We present a neural Bayes estimator (NBE) for key epidemic quantities: the reproduction number, prevalence, and cumulative infections through time. By performing quantile regression over tree space, the NBE allows us to estimate posterior medians and credible intervals directly from a reconstructed tree. Our approach uses a recursive neural network as a tree embedding network with a prediction network conditioned on time and quantile level to generate the estimates. In simulation studies, the NBE achieves good predictive performance, with conservative uncertainty estimates. Compared with a BEAST2 fixed-tree analysis, the NBE gives less biased estimates of time-varying reproduction numbers in our test setting. Under a misspecified sampling model, the NBE performance degrades (as expected) but remains reasonable, and fine-tuning a pre-trained model yields estimates comparable to those from a model trained from scratch, at substantially lower computational cost.

*Corresponding author: aezarebski@gmail.com

1 Introduction

In this paper we consider the birth-death-sampling model of an epidemic: infections generate (give birth to) new lineages, infected individuals become uninfected and a lineage ends (death), and a subset of these “becoming uninfected events” involve sequencing of the pathogen (sampling). The observed (sampled) infections then form the tips of a reconstructed viral phylogeny (hereafter the tree).

In Fig. 1 we illustrate the difference between the (latent) *transmission tree* and the *reconstructed tree* obtained from a set of sequenced samples. Our goal is to estimate time-varying epidemic quantities from the reconstructed tree, in particular the effective reproduction number, \mathcal{R} ; the common logarithm of the prevalence of infection, $\log_{10}(N_p)$ (where N_p is the number of extant lineages in the transmission tree at a given time); and the common logarithm of the cumulative number of infections, $\log_{10}(N_c)$ (where N_c is the number of transmission events prior to a given time). These quantities are central for understanding transmission, evaluating control measures, and contextualizing genomic surveillance data.

Likelihood-based Bayesian phylodynamic methods (e.g. those typically performed with BEAST X (Baele et al., 2025) or BEAST2 (Bouckaert et al., 2019)) provide a principled framework for joint inference of trees and epidemiological parameters, but often require evaluating complex likelihoods which hampers progress (Voznica et al., 2022). In practice, inference is often limited by the cost of repeatedly evaluating complex likelihoods and exploring high-dimensional posteriors via MCMC. Moreover, scaling to large genomic datasets may require careful approximation, strong model simplifications or substantial computational resources (Zarebski et al., 2022; Zarebski et al., 2025).

Recent work has explored *amortized* methods based on deep learning, as an alternative to MCMC based approaches (Zammit-Mangion et al., 2025). In neural approaches to amortized inference a neural network is trained to map data to estimates. Since the resulting models are usually fast to evaluate they can rapidly generate estimates for new datasets. For example, Voznica et al., 2022 introduces *PhyloDeep* for parameter estimation using a fixed-size vectorization: the compact bijective ladderized vector (CBLV). To avoid identifiability issues, Voznica et al., 2022 provide the sampling probability as input to the network. An alternative to the CBLV is *Phylo2Vec* (Penn et al., 2024) tree embedding which could be extended to account for branch lengths.

The approach of representing trees using hand-crafted encodings has some limitations. Often lineages that are close in the tree may be encoded in distant parts of the encoding, potentially diluting local structure across a large receptive field;

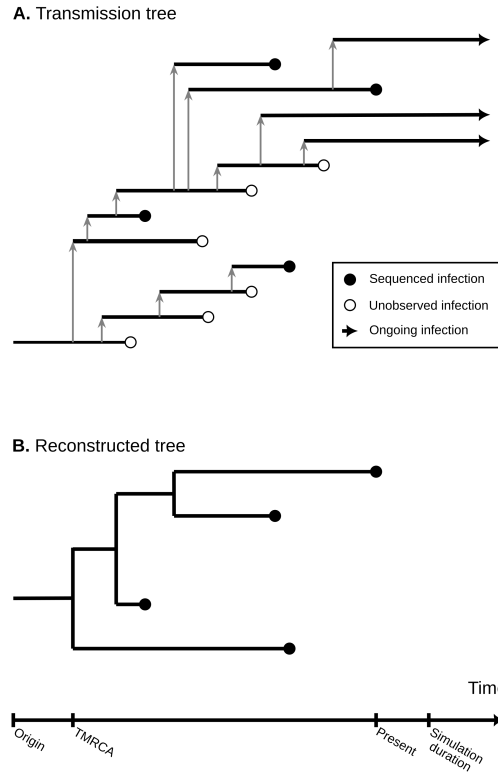


Figure 1: The transmission process is modeled as a birth-death process, in which the transmission of the pathogen is represented by the birth of a new lineage, and the end of an infectious period is represented by the death of a lineage. **A.** The transmission tree is a complete description of the transmission and observation processes. Starting from a single infectious individual, new infections are indicated with grey arrows, and an infection may end with the pathogen genome sequenced (filled dot). At the end of this example, there is a prevalence of three ongoing infections and the cumulative number of infections is 13. **B.** The reconstructed tree describes the connections between the sequenced infections. The time of the final sequenced infection is designated as the present.

it imposes a bounded input size, requiring padding for smaller trees and splitting or subsampling for larger trees; and because estimation operates on a fixed vectorization, extending the method to other tasks, such as labeling internal nodes, is non-trivial. Moreover, much of the existing deep-learning work in this area has focused on models with constant rates, and uncertainty quantification is frequently obtained via variants of the parametric bootstrap, which requires additional simulation at prediction time (Voznica et al., 2022; Lambert et al., 2023).

The literature mentioned above suggests several practical gaps for amortized,

simulation-based estimators in phylodynamics. First, many approaches rely on fixed-size tree encodings, which complicate the use of variable-size trees and the inclusion of additional metadata. Second, quantities that change over time (such as $\mathcal{R}(t)$) are often of interest, for example, to assess the impact of particular interventions. However, estimation of time-varying quantities have received less attention in deep-learning-based approaches. Third, efficient uncertainty quantification remains challenging: many methods require additional simulation (e.g. bootstrap-style procedures) to obtain intervals, which reduces the computational advantages of amortization. Finally, applied work frequently needs multiple outputs (e.g. reproduction number, prevalence, and cumulative incidence), ideally inferred in a single, consistent framework.

Other architectures have been proposed, including graph neural networks (GNNs) and recurrent neural networks. Comparisons have highlighted that GNNs can perform poorly in phylodynamic settings if not configured appropriately (Lajaaiti et al., 2023), motivating tailored pooling schemes and architectural refinements (Leroy et al., 2025). Taken together, these developments motivate a need for methods that (i) preserve tree structure, (ii) naturally extend to trees of any size, (iii) support time-varying quantities, and (iv) provide calibrated uncertainty with minimal additional computation.

We address these gaps with a neural Bayes estimator (NBE) trained via simulation-based inference under a birth-death-sampling generative model. The estimator takes as input a reconstructed phylogeny \mathcal{T} and an estimate of the mean infectious duration σ^{-1} , and returns *quantiles* of the posterior distribution of $\mathcal{R}(t)$, $\log_{10}(N_p(t))$, and $\log_{10}(N_c(t))$ at user-specified times t and quantile levels $\tau \in [0, 1]$. A single trained model can produce posterior marginal medians and credible intervals without running MCMC or performing additional bootstrap simulations at prediction time.

The approach we take to learning a useful embedding of trees makes use of a recursive neural network (RvNN), (Frasconi et al., 1998). The RvNN generates tree embeddings by propagating information from tips to the root, producing a fixed-length embedding of the full tree. This embedding is then combined with a feed-forward prediction network along with the time and quantile level to produce the desired estimates. As we demonstrate below, separating the networks into an embedding and a prediction network enables the embedding component to be re-used in other estimation problems with only minor fine-tuning. We assume the reconstructed tree is observed without error and that σ is available (or can be estimated externally), which is not unusual in applied work. For example a tree may be obtained via maximum likelihood or parsimony methods and clinical information about infectious periods, such as the mean generation time, may be

available.

Our RvNN architecture annotates each internal node with an embedding of its descendant lineages, avoiding ad hoc padding or splitting and offering substantial flexibility. Beyond learning a useful embedding, we incorporate quantile regression directly into the amortized estimator, enabling prediction of arbitrary posterior quantiles (and hence credible intervals) without additional simulation. Finally, by conditioning on time t we obtain a single model that can be queried to produce trajectories of $\mathcal{R}(t)$, $\log_{10}(N_p(t))$, and $\log_{10}(N_c(t))$ across the epidemic.

In §2 we describe the NBE and how it was trained: in §2.1 we describe the birth-death-sampling model used to simulate the data, in §2.2 we describe the neural network architecture used in the NBE to generate estimates, and in §2.3 we describe how the NBE was trained. In §3 we report the results of computational experiments: in §3.1 we describe a simulation study assessing the calibration of the NBE’s estimates, in §3.2 we compare the NBE’s estimates of the reproduction number to those generated with using MCMC, specifically a BEAST2 analysis using BDSky, and in §3.3 we carry out a sensitivity analysis of how the NBE performs when the sampling model is misspecified, and demonstrate how fine-tuning offers a solution to overcoming issues of this nature. §4 offers some discussion on the use of NBEs in phylodynamic inference.

2 Methods

2.1 Birth-death-sampling model

The generative model we consider is a birth-death-sampling model (Stadler et al., 2024) with (random) piece-wise constant functions used for the parameters for the reproduction number, \mathcal{R} , and the proportion of infections that end in sequencing, p_ψ ; and a (randomly sampled) constant for the net rate of becoming uninfected, σ . Further details of the generative model are provided in §SI7.1. The prior distribution over the parameters is detailed in Tab. SI4; the prior is based on one used for an analysis of SARS-CoV-2 transmission (Douglas et al., 2021).

We assume that a tree, \mathcal{T} , can be reconstructed without error from the sequenced samples in the simulation, and that the average duration of being infectious, or equivalently, the net becoming-uninfected rate, σ is known. Given an observation of (\mathcal{T}, σ) , we are interested in the posterior distribution of three quantities throughout the course of the epidemic: the reproduction number, \mathcal{R} , the common logarithm of the prevalence of infection, $\log_{10}(N_p)$, and the common

logarithm of the cumulative number of infections, $\log_{10}(N_c)$. Since the prevalence and cumulative number of infections can vary over several orders of magnitude, we consider the common logarithm (with base 10) of these quantities rather than their value directly.

2.2 Neural Bayes estimator

Neural amortized inference methods have been developed to avoid running expensive likelihood-based MCMC analyses from scratch for every new dataset (Zammit-Mangion et al., 2025). Neural Bayes estimators (NBEs) use neural networks to approximate Bayes estimators (Sainsbury-Dale et al., 2024). NBEs, and similar methods, use simulated data to train a neural network that maps an observed tree directly to parameter estimates (Voznica et al., 2022). Our neural Bayes estimator (NBE) performs quantile regression over tree space for the marginal posterior quantities of interest. The required function is $f : \mathbb{T} \times \mathbb{R}_{>0} \times \mathbb{R}_{\geq 0} \times [0, 1] \rightarrow \mathbb{R}^3$ such that

$$f(\mathcal{T}, \sigma^{-1}, t, \tau) = (Q_{\text{prev}}(\tau), Q_{\text{cuminc}}(\tau), Q_{\text{Reff}}(\tau))$$

where $\mathcal{T} \in \mathbb{T}$ is the tree reconstructed from the sequenced samples, $\sigma^{-1} \in \mathbb{R}_{\geq 0}$ is the average duration of infectiousness, $t \in \mathbb{R}_{\geq 0}$ indicates the time in the process we are interested in, and $\tau \in [0, 1]$ indicates the desired quantile. The $Q_{\text{prev}}(\tau)$, $Q_{\text{cuminc}}(\tau)$, and $Q_{\text{Reff}}(\tau)$ are the quantile functions of the posterior (predictive) distributions of the (common logarithm of the) prevalence and cumulative incidence, and reproduction number. Given f we can compute posterior medians and marginal credible intervals for $\log_{10}(N_p(t))$, $\log_{10}(N_c(t))$ and $\mathcal{R}(t)$.

Since we cannot obtain the function f directly, we will approximate it with a neural network f_{NBE} :

$$f(\mathcal{T}, \sigma^{-1}, t, \tau) \approx f_{\text{NBE}}(\mathcal{T}, \sigma^{-1}, t, \tau) = f_{\text{pred}}(f_{\text{BTU}}(\mathcal{T}), \text{HEIGHT}(\mathcal{T}), \sigma^{-1}, t, \tau)$$

where f_{BTU} and f_{pred} are two neural networks as described below (in §2.2.1 and §2.2.2 respectively), and HEIGHT returns the tree’s height. The parameters of f_{NBE} are the parameters of the subnetworks f_{BTU} and f_{pred} described below.

2.2.1 Binary tree unit

The function f_{BTU} is the *binary tree unit* (BTU), a recursive neural network (RvNN) (Frasconi et al., 1998). RvNN describe functions on directed acyclic graphs of bounded degree and size, but we only consider the special case of binary

trees with weighted edges. Here we consider the definition of a f_{BTU} which embeds a tree \mathcal{T} into \mathbb{R}^n for a given n .

Before defining f_{BTU} , it is helpful to define some functions on the set of trees. Note that for some of these functions, (e.g. DEPTH), there is an implicit supertree that we have omitted to simplify the presentation. Let \mathbb{T} denote the set of binary trees (with branch lengths) and $\mathbb{T}_1 \subset \mathbb{T}$ the subset of trees which are a single leaf.

- LEFT (and RIGHT) : $\mathbb{T}/\mathbb{T}_1 \rightarrow \mathbb{T}$ extracts the left (or right) subtree of a given tree
- BRANCH : $\mathbb{T} \rightarrow \mathbb{R}_{\geq 0}$ extracts the length of the branch connecting a tree to its parent, for a root this is defined to be zero.
- DEPTH : $\mathbb{T} \rightarrow \mathbb{R}_{\geq 0}$ returns the depth of the root node of the given tree (within a supertree).
- HEIGHT : $\mathbb{T} \rightarrow \mathbb{R}_{\geq 0}$ returns the height of a given tree.

With these functions we can then define $f_{\text{BTU}} : \mathbb{T} \rightarrow \mathbb{R}^n$ in the following way:

$$f_{\text{BTU}}(\mathcal{T}) = \begin{cases} \sigma([\text{DEPTH}(\mathcal{T})/h_{\text{super}}, \text{BRANCH}(\mathcal{T})/h_{\text{super}}, \mathbf{0}]), & \text{if } \mathcal{T} \in \mathbb{T}_1 \\ g([\sigma([\text{DEPTH}(\mathcal{T})/h_{\text{super}}, \text{BRANCH}(\mathcal{T})/h_{\text{super}}]), & \text{otherwise} \\ f_{\text{BTU}}(\text{LEFT}(\mathcal{T})), \\ f_{\text{BTU}}(\text{RIGHT}(\mathcal{T}))]) \end{cases} \quad (1)$$

where $g : \mathbb{R}^{2n+2} \rightarrow \mathbb{R}^n$ is a neural network with activation function σ , $\mathbf{0}$ is a vector of $n - 2$ zeros and h_{super} is the height of the supertree for the given tree. We used a multilayer perceptron (MLP) for g with 2 hidden layers of width 50 (i.e. we are embedding trees into \mathbb{R}^{50}) with the exponential linear unit (ELU) activation function (Clevert et al., 2015).

In the definition of f_{BTU} , we normalized both the node depth and branch lengths by the supertree height to ensure they take values from zero to one. Due to the scaling of branch lengths and depths by the height of the tree the BTU learns an embedding of trees that is invariant of the scaling of the tree. This is important as it means that the embedding does not depend upon the *absolute* time scale.

2.2.2 Prediction unit

The function f_{pred} is the prediction unit, $f_{\text{pred}} : \mathbb{R}^n \times \mathbb{R}_{>0} \times \mathbb{R}_{>0} \times \mathbb{R}_{\geq 0} \times [0, 1] \rightarrow \mathbb{R}^3$, defined as

$$f_{\text{pred}}(r_{\mathcal{T}}, t_h, \tilde{\sigma}^{-1}, \tilde{t}_m, \tau) = h([r_{\mathcal{T}}, t_h, \tilde{\sigma}^{-1}, \tilde{t}_m, \tau]) \quad (2)$$

where $h : \mathbb{R}^{n+4} \rightarrow \mathbb{R}^3$ is a neural network returning the quantiles for \mathcal{R} , $\log_{10}(N_p)$, and $\log_{10}(N_c)$; $r_{\mathcal{T}} = f_{\text{BTU}}(\mathcal{T})$ is the embedding of the reconstructed tree from the BTU; $t_h = \text{HEIGHT}(\mathcal{T})$ is the height of the reconstructed tree (because there needs to be some time scale information); $\tilde{\sigma}^{-1}$ is the average infection duration scaled by the height of \mathcal{T} ; and \tilde{t}_m is the measurement time, again scaled by the height of the input tree. We used an MLP for h with 2 hidden layers of width 100 and ELU activations. When generating the predictions, we applied a softplus activation to get the \mathcal{R} estimate, to ensure it is positive.

2.3 Data and training

2.3.1 Loss function

To learn the quantiles of the posterior distribution we used the *pinball loss function* (a.k.a. the *tilted absolute value loss function*) (Zammit-Mangion et al., 2025), for a given quantile τ , the pinball loss ℓ_{τ} is given by

$$\ell_{\tau}(\hat{y}, y) = \begin{cases} \tau(y - \hat{y}) & \text{if } y \geq \hat{y} \\ (1 - \tau)(\hat{y} - y) & \text{otherwise.} \end{cases}$$

To learn all of the quantiles simultaneously, we take the expected loss summed over the three of the quantities of interest. We approximate the expectation with the Monte Carlo estimate:

$$\mathbb{E}_{y, \tau}[\ell_{\tau}(\hat{y}, y)] \approx \frac{1}{IJ} \sum_{I=1}^I \sum_{j=1}^J \sum_{k=1}^3 \ell_{\tau_i}(\hat{y}_{i,j,k}, y_{i,j,k}) \quad (3)$$

for a batch of I simulations, each of which has J measurements, where τ_i and $y_{i,j,k}$ are sampled from the prior distribution with $y_{i,j,k}$ the measurement of the k th quantity at the j th observation time in the i th simulation.

2.3.2 Optimization

The NBE was optimized using AdamW (Loshchilov and Hutter, 2017) using the default parameters in PyTorch (e.g. a learning rate of 10^{-3}). We used batches

of 32 simulations, each with measurements at 128 points in time throughout the simulation. For each batch, we used a different value of $\tau_i \sim \text{Beta}(0.5, 0.5)$ in Eq. (3). We used simple early stopping, selecting the state of the model with the lowest validation error across the training epochs. All model weights and biases were initialized using the default method in PyTorch, excluding the last layer of the prediction unit where we initialized the bias to match the sample average of the training data and set the weights to zero. During training, we used dropout on internal layers with 10% of nodes zeroed out. All of the network optimization was carried out on CPUs comparable to what would be available in a mid-range desktop.

2.3.3 Simulating training and testing data

The training data for our NBE was simulated from the model described above. A more detailed description of the data generation process is given in §SI7.1. Each simulation produces a reconstructed tree of sampled infections, a value of the net becoming-uninfectious rate, and measurements (through time) of the three quantities. I.e. at time t in the simulation, we measure $(\mathcal{R}(t), \log_{10}(N_p(t)), \log_{10}(N_c(t)))$. These measurements are taken at 128 randomly sampled times between the beginning of the process and the randomly sampled stopping time. The training dataset has 8,000 simulations, with a further 1,000 each for validation and testing.

3 Results

3.1 Simulation study

Using the simulation and training procedure described above, we trained an NBE to predict time-varying epidemic quantities from reconstructed trees. In Fig. SI4 we show the training and validation loss throughout training. We use the model weights with the lowest validation loss across the 500 training epochs. Below we describe our assessment of the predictive performance and calibration of this trained model on the held-out testing simulations.

In Fig. 2 we show the NBE estimates (and 95% credible intervals) of the reproduction number, \mathcal{R} , and the common logarithm of prevalence, $\log_{10}(N_p)$, and cumulative incidence, $\log_{10}(N_c)$, for a randomly sampled time in each of the 1,000 testing simulations. The estimates of the prevalence of infection and the cumulative number of cases is very good (over 95% of the variance is explained

with little bias). On average the estimates for the reproduction number are good (approximately 90% of the variance is explained with little bias).

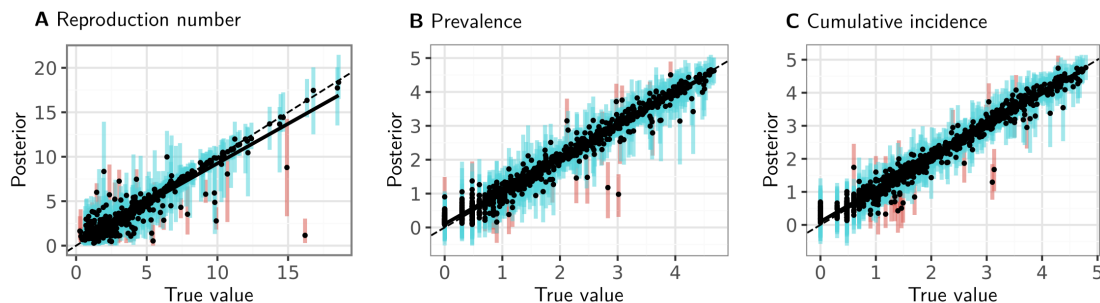


Figure 2: The predictions and 95% confidence intervals on the testing data for the three prediction targets **A** the reproduction number, **B** the (common logarithm of the) prevalence of infection, and **C** the (common logarithm of the) cumulative number of infections. The bars associated with each point are blue if the estimated credible interval contains the true value and red otherwise. The dashed black line indicates perfect agreement and the solid black line is a least squares fit.

In Tab. 1 we summarize the performance across the 128 measurements for each of the 1,000 testing trees. The uncertainty in the predictions of the reproduction number appears to be well-calibrated, if slightly pessimistic: the credible intervals, in particular the 50% credible intervals, are too large. As an indication of the range of values expected of a well-calibrated estimate, in a hypothesis test with a 0.05 level of significance, for the 50% intervals, the acceptable range would cover 0.469–0.531; and for the 95% intervals, the acceptable range would cover 0.936–0.963.

Quantity	R^2	Bias	Cover. 50%	Cover. 95%
Reproduction number, \mathcal{R}	0.881	-0.020	0.690	0.959
Prevalence, $\log_{10}(N_p)$	0.966	0.047	0.606	0.968
Cumulative incidence, $\log_{10}(N_c)$	0.971	0.045	0.604	0.966

Table 1: Summary statistics for the estimates from the NBE over 1,000 trees, each quantity being measured at 128 different times throughout the simulation. R^2 is the coefficient of determination, the proportion of the variance explained. Coverage at X% indicates the proportion of X% credible intervals that contained the true value from the simulation.

3.2 Comparison to existing method

Using the same trained NBE considered in §3.1, we carried out a comparison of the NBE’s estimates with those generated by MCMC with BEAST2 using the

BDSky tree prior with a fixed (known) tree. In Fig. 3 we show an example of the estimate of the effective reproduction number through time generated with the NBE and the corresponding estimates generated with the MCMC methods. The BDSky tree prior used in the MCMC is misspecified. The simulated testing data uses a randomly sampled piece-wise constant function with two or three pieces that change at random times for both the reproduction number and the sampling proportion; the model in the MCMC assumes a constant sampling proportion and a piece-wise constant reproduction number that changes at 9 points.

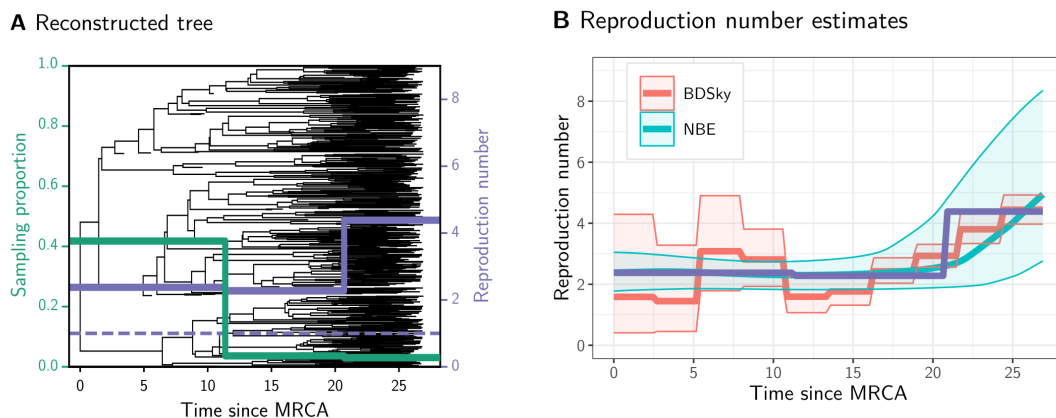


Figure 3: Example of a realization of the birth-death sampling process and the estimates of the reproduction number generated for this data using both MCMC and NBE. **A.** The simulated tree and the varying reproduction number and proportion of infections sampled through time. **B.** Estimates of the effective reproduction number produced by BDSky MCMC and the NBE and their 95% credible intervals along with the true value. The NBE estimates do not make a piece-wise constant assumption, so they vary smoothly through time, whereas the MCMC uses a piece-wise constant estimator.

To compare the performance of our neural estimator to that of a gold-standard BDSky MCMC method, we considered the performance of a fixed-tree BDSky analysis (Stadler et al., 2013) with BEAST2 (Bouckaert et al., 2019) across the 1,000 testing simulations. Details of the MCMC analysis are provided in the §SI7.3.

In Tab. 2 we show the results of this comparison: the NBE explains more of the variability (as measured by the coefficient of determination, R^2) and is less biased. The coverage of the credible intervals is greater for the NBE than the BDSky MCMC. At both 50% and 95% the NBE coverage exceeds the desired coverage, while for the MCMC it is smaller than the desired level. This is likely due to the model misspecification between the model used in the MCMC and the model used to simulate the testing data. Note that a small proportion of estimates are missing

from the MCMC analysis because if a measurement time falls before the TMRCA or after the most recent sample (see Fig. 1) then there is no estimate generated for that measurement.

Method	R^2	Bias	Cover. 50%	Cover. 95%	Time (sec)
NBE	0.881	-0.020	0.690	0.959	0.167
MCMC	0.763	-0.348	0.464	0.906	23.3

Table 2: Comparison of estimates of the reproduction number through time generated by the NBE and a BEAST2 MCMC analysis using BDSky. These metrics are computed from the analysis of the estimates at 128 times in the 1,000 testing simulations using both the NBE and MCMC (with BEAST2). The values in Time for the MCMC analysis are the average number of seconds required to attain an effective sample size (ESS) of 200 for all variables. The NBE outperforms the MCMC on most of the considered metrics, (**bold** indicates the best value for each metric.)

3.3 Sensitivity analysis

The practical utility of an amortized estimator depends on its ability to generalize beyond the precise assumptions used to generate the training data. We evaluate sensitivity to model assumptions in two ways: in §3.3.1, we consider misspecification of the observation model; and in §SI7.2.2, we report qualitatively similar results from an additional analysis of sensitivity to prior misspecification.

3.3.1 Model misspecification

To understand the NBE’s performance under model misspecification, we simulated a second, alternative dataset. This alternative dataset (described in more detail in §SI7.2.1) is simulated from a process in which initially there is no sampling, and then after a random time sampling is activated. This is a plausible scenario to consider, for example, it could correspond to an initial period in which the pathogen is spreading before it has come to the attention of the surveillance system. As in §2.3.3, we split this alternative data into training, validation and testing datasets.

Using both this new dataset, and the original one described above, we trained the three models described below, in each case running the optimizer as described above for 250 epochs: **zero-shot**, in which we take the model trained on the original training dataset for 250 epochs without modification; **fine-tuning**, in which we take the model trained on the original training dataset (i.e. the zero-shot

model) and fine-tune the prediction unit on the alternative training dataset; and **random initialization**, in which we train a model from random initialization on the alternative training dataset (using the alternative validation dataset for early stopping).

In Tab. 3 we summarize the performance of the three models on the alternative testing dataset. The first row demonstrates that the fine-tuning process is several orders of magnitude faster than training the full model. The performance of the fine-tuned model is very similar to that of the model trained from random initialization.

		Zero-shot pre-trained	Fine-tuned pre-trained	Randomly initialized
Training time	seconds	0	<u>215</u>	242978
Reproduction number	R^2 95% cover.	0.692	0.754	<u>0.742</u>
Prevalence of infection	R^2 95% cover.	0.956	0.969	<u>0.965</u>
Cumulative infections	R^2 95% cover.	0.951	0.965	<u>0.962</u>
		94	96	96
		91	<u>96</u>	95

Table 3: Fine-tuning a pre-trained model is much faster than training a new model and recovers much of the performance lost to model misspecification. The coefficient of determination, R^2 , and coverage of the 95% credible interval is shown for each model and quantity. The **bold** entry is the best in each row, with the second best underlined. The training time of the zero-shot model is zero because we assume there is a pre-trained model to be used in this case and fine-tuned in the fine-tuning example.

4 Discussion

Neural Bayes estimators (NBEs) can estimate important quantities of an epidemic using a reconstructed phylogeny as data. The quantities we consider here are the *time varying* effective reproduction number, prevalence of infection, and cumulative number of infections. This represents an important extension of capability because standard MCMC methods typically only estimate either the effective reproduction number or (a quantity proportional to) the prevalence of infection, and other simulation-based inference (SBI) methods are computationally expensive when they are not completely intractable. Importantly, the NBE method we present here can be trained without expensive hardware (e.g., GPUs), and our

simulation studies (§3.1) suggest the resulting estimators have little bias and conservative uncertainty, with interval coverage generally at or above nominal levels.

To understand how the NBEs perform relative to a gold-standard MCMC method (e.g., a fixed-tree BDSky analysis with BEAST2), we performed a simulation study comparing NBE estimates to those from MCMC (§3.2) for the effective reproduction number. We found that NBEs outperform the MCMC on point-estimate accuracy and bias in this simulation setting. Importantly, once trained, the NBEs are at least an order of magnitude faster than the MCMC methods. This speedup is typical with neural inference methods (Zammit-Mangion et al., 2025). We did not compare performance on the estimation of prevalence and cumulative infections because there is no definitive standard method for this problem yet.

The ability of neural networks to generalize beyond their training data is a major concern in their practical application. We performed a sensitivity analysis (§3.3 and §SI7.2.2), to assess the NBE’s performance under model misspecification. The main observations of this experiment are that, as expected, performance degrades with a misspecified model, however the NBE still generates reasonable estimates, and, with a small amount of fine-tuning (which is computationally cheap), a pre-trained model can achieve comparable performance to one that was trained from scratch using data simulated from the true model. This observation supports the notion that if one wanted to use a prior or model that differed substantially from the one the NBE was trained with, this could be done with little additional computational cost. This observation is important as it builds confidence these neural estimators will perform as desired when used on real data and are extensible to novel settings.

An additional observation related to the fine-tuning simulation studies (§3.3 and §SI7.2.2) is that the good performance of the fine-tuned pre-trained model suggests the NBE has learned a useful tree embedding. This is significant as it suggests the NBE could be used as a foundation model, reducing the computational cost associated with training subsequent NBEs for phylodynamic estimation.

NBEs offer a conceptually simple way to estimate a range of quantities, without needing to derive complicated likelihoods, algorithms to compute them, or informative summary statistics. This enables the user to focus on their model and the questions they are interested in answering, rather than the complexity of likelihood derivations.

While NBEs have a significant cost associated with simulation and training, the computational cost of inference is negligible. With sensitive data increasingly stored on trusted research environments/secure data enclaves, this allocation of computational costs is increasingly beneficial; if necessary, the simulation and

training steps can be carried out on HPC servers and the resulting model transferred to a lower-powered machine for inference on the sensitive real data. In comparison, particle-based methods and ABC place the computational cost on the inference step, and this must be paid each time a new observed dataset is considered. As mentioned above, the computation performed for this study was all done without the use of an HPC cluster or specialized hardware such as GPUs, suggesting it will be viable for many practitioners with limited resources.

There are two main weaknesses of this work that we discuss below: the first is that the estimators rely on a reconstructed tree as input, so the estimates do not account for tree uncertainty; the second is that unlike likelihood-based methods (e.g. most gold-standard MCMC approaches), it is not obvious how these estimators will generalize beyond the scope of their training data.

There are several ways to overcome the requirement for a reconstructed tree. One approach is to avoid the tree entirely by using a multiple sequence alignment (MSA) transformer (Rao et al., 2021), which works on an MSA directly without the need to estimate a tree — although this does still require an MSA to be produced, so it doesn't entirely solve the problem of a substantial amount of preprocessing being involved. Overcoming the lack of uncertainty in the reconstructed tree could be done (in a birth-death Bayesian setting) by applying the neural estimator to a posterior sample of trees and sampling from the implicit distributions over the prevalence and cumulative incidence to draw a sample from the posterior predictive distribution for these quantities. (The effective reproduction number would already have been sampled in generating the trees in the typical analysis.)

Understanding the generalization properties of NBEs is a substantial problem. While it is possible to force the NBE estimates to respect certain constraints by encoding them in the neural network architecture, this does not ensure the NBE's performance will be maintained. Until we have a better understanding of these properties, we advise some caution in the use of NBEs, for example, by checking that summary statistics of the observed data fall within the distribution of those statistics across the training data, although there are more formal approaches to this as well, cf., Tagasovska and Lopez-Paz, 2019. Of course, model adequacy is an entirely separate problem for which we recommend prior and posterior simulation, which is an important part of the Bayesian workflow (Gelman et al., 2020).

There are three particularly interesting extensions to the current work that would further enhance the utility of these methods. The first is to reduce the main computational cost: simulating the training data, which could be done using emulation methods (Scheurer et al., 2025). The second is to use normalizing flows to estimate the full joint posterior distributions rather than marginal predic-

tions (Radev et al., 2022). Finally, the third would be to gain better diagnostics for when a particular NBE is not appropriate by detecting when a new data point sits outside of the training data (Tagasovska and Lopez-Paz, 2019).

The work we present here shows recursive neural networks offer a powerful tool for representation learning of trees, and that NBEs can use reconstructed trees to quickly estimate key epidemic trajectories with quantified uncertainty. In our simulation studies, the NBEs are competitive with an MCMC baseline for estimating the effective reproduction number, and NBEs remain useful under model misspecification when fine-tuning is used. Taken together, these results support amortized phylodynamic inference as a useful addition to traditional likelihood-based Bayesian workflows, particularly for complex models.

5 Data availability

An implementation of the NBE along with the code to simulate the training data and train the neural networks are linked to from the project homepage: <https://aezarebski.github.io/derp/>.

6 Acknowledgments

AEZ acknowledges support from the Wellcome Trust [grant number 227438/Z/23/Z], and an Andrew Sisson Early Career Researcher grant. TW acknowledges funding through the ARC Centre of Excellence for the Mathematical Analysis of Cellular Systems, and was supported by internal funding from The University of Melbourne, School of Mathematics & Statistics.

References

- Baele, Guy et al. (2025). “BEAST X for Bayesian phylogenetic, phylogeographic and phylodynamic inference”. In: *Nature Methods* 22.8, pp. 1653–1656. DOI: 10.1038/s41592-025-02751-x.
- Bouckaert, Remco et al. (Apr. 2019). “BEAST 2.5: An advanced software platform for Bayesian evolutionary analysis”. In: *PLOS Computational Biology* 15.4, pp. 1–28. DOI: 10.1371/journal.pcbi.1006650.

- Clevert, Djork-Arné, Thomas Unterthiner, and Sepp Hochreiter (Nov. 2015). “Fast and Accurate Deep Network Learning by Exponential Linear Units (ELUs)”. In: *arXiv e-prints*. DOI: 10.48550/arXiv.1511.07289.
- Douglas, Jordan et al. (June 2021). “Phylodynamics reveals the role of human travel and contact tracing in controlling the first wave of COVID-19 in four island nations”. In: *Virus Evolution* 7.2, veab052. DOI: 10.1093/ve/veab052.
- Frasconi, P., M. Gori, and A. Sperduti (1998). “A general framework for adaptive processing of data structures”. In: *IEEE Transactions on Neural Networks* 9.5, pp. 768–786. DOI: 10.1109/72.712151.
- Gelman, Andrew et al. (Nov. 2020). “Bayesian Workflow”. In: *arXiv e-prints*. DOI: 10.48550/arXiv.2011.01808.
- Lajaaiti, Ismaël et al. (2023). “A Comparison of Deep Learning Architectures for Inferring Parameters of Diversification Models from Extant Phylogenies”. In: *bioRxiv*. DOI: 10.1101/2023.03.03.530992.
- Lambert, Sophia, Jakub Voznica, and Hélène Morlon (Aug. 2023). “Deep Learning from Phylogenies for Diversification Analyses”. In: *Systematic Biology* 72.6, pp. 1262–1279. DOI: 10.1093/sysbio/syad044.
- Leroy, Amélie et al. (2025). “Graph Neural Networks for Likelihood-Free Inference in Diversification Models”. In: *bioRxiv*. DOI: 10.1101/2025.08.14.670341.
- Loshchilov, Ilya and Frank Hutter (Nov. 2017). “Decoupled Weight Decay Regularization”. In: *arXiv e-prints*. DOI: 10.48550/arXiv.1711.05101.
- Penn, Matthew J et al. (June 2024). “Phylo2Vec: A Vector Representation for Binary Trees”. In: *Systematic Biology* 74.2, pp. 250–266. DOI: 10.1093/sysbio/syae030.
- Radev, Stefan T. et al. (2022). “BayesFlow: Learning Complex Stochastic Models With Invertible Neural Networks”. In: *IEEE Transactions on Neural Networks and Learning Systems* 33.4, pp. 1452–1466. DOI: 10.1109/TNNLS.2020.3042395.
- Rao, Roshan M et al. (July 2021). “MSA Transformer”. In: *Proceedings of the 38th International Conference on Machine Learning*. Ed. by Marina Meila and Tong Zhang. Vol. 139. Proceedings of Machine Learning Research. PMLR, pp. 8844–8856.
- Sainsbury-Dale, Matthew, Andrew Zammit-Mangion, and Raphaël Huser (2024). “Likelihood-Free Parameter Estimation with Neural Bayes Estimators”. In: *The American Statistician* 78.1, pp. 1–14. DOI: 10.1080/00031305.2023.2249522.
- Scheurer, Stefania et al. (May 2025). “Uncertainty-Aware Surrogate-based Amortized Bayesian Inference for Computationally Expensive Models”. In: *arXiv e-prints*. DOI: 10.48550/arXiv.2505.08683.
- Stadler, Tanja et al. (2013). “Birth-death skyline plot reveals temporal changes of epidemic spread in HIV and hepatitis C virus (HCV)”. In: *Proceedings of*

- the National Academy of Sciences* 110.1, pp. 228–233. DOI: 10.1073/pnas.1207965110.
- Stadler, Tanja et al. (Apr. 2024). *Decoding Genomes: From Sequences to Phylogenetics*. ETH Zurich. DOI: 10.3929/ethz-b-000664449. URL: <https://decodinggenomes.org/>.
- Tagasovska, Natasa and David Lopez-Paz (2019). “Single-model uncertainties for deep learning”. In: *Advances in Neural Information Processing Systems*. Vol. 32. DOI: 10.48550/arXiv.1811.00908.
- Voznica, J. et al. (July 2022). “Deep learning from phylogenies to uncover the epidemiological dynamics of outbreaks”. In: *Nature Communications* 13.1, p. 3896. DOI: 10.1038/s41467-022-31511-0.
- Zammit-Mangion, Andrew, Matthew Sainsbury-Dale, and Raphaël Huser (2025). “Neural Methods for Amortized Inference”. In: *Annual Review of Statistics and Its Application* 12, pp. 311–335. DOI: 10.1146/annurev-statistics-112723-034123.
- Zarebski, Alexander E. et al. (Feb. 2022). “A computationally tractable birth-death model that combines phylogenetic and epidemiological data”. In: *PLOS Computational Biology* 18.2. DOI: 10.1371/journal.pcbi.1009805.
- Zarebski, Alexander E. et al. (June 2025). “Estimating epidemic dynamics with genomic and time series data”. In: *Journal of The Royal Society Interface* 22.227. DOI: 10.1098/rsif.2024.0632.

7 Supplementary Information

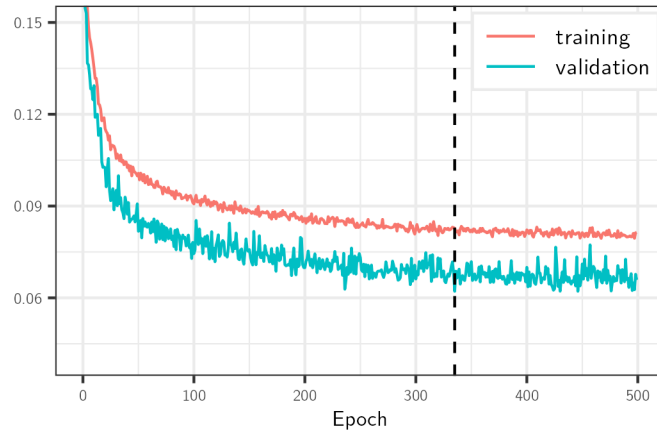


Figure 4: Learning curves show that the training and validation losses across epochs have effectively converged by epoch 500. The validation loss is less than the training loss because drop-out was applied when assessing the training loss. The vertical dashed line indicates the epoch with the lowest validation loss.

7.1 Simulation

Each simulation in our database is obtained by sampling parameters from a prior distribution and then sampling from a birth-death-sampling process with those parameters. The details of this process are enumerated below, and we summarize the distributions used in Tab. SI4. The prior distribution on the model parameters is adapted from an analysis of SARS-CoV-2 genomes in Douglas et al., 2021.

1. Sample a stopping time for the simulation of 30–90 days:

$$T_{\text{stop}} \sim \text{Discrete-uniform}\{30, \dots, 90\}.$$

2. Sample a constant net becoming-uninfectious rate from a log-normal distribution: $\sigma \sim \text{lognormal}(-1.81, 0.2)$. This prior has been scaled from the one used in Douglas et al., 2021 to be in units of days (rather than years).
3. Sample random change points for the piece-wise constant functions by first drawing a number of change points from a discrete-uniform distribution on 1, 2, and then sampling that number of change times from the distribution $U(0, T_{\text{stop}})$.

4. Sample the values for the piece-wise constant function describing the reproduction number, $\mathcal{R} \sim \text{lognormal}(1.0, 0.7)$
5. Sample the values of the piece-wise constant proportion of infections that are observed, $p_\psi \sim \text{Beta}(1.1, 8.0)$. It is this part of the process that is changed in the alternative simulation described in §SI7.2.1.
6. Compute the birth, death and sampling rates, λ , μ and ψ as piece-wise constant functions from the sampled values of \mathcal{R} , σ and p_ψ .
7. Sample from the birth-death-sampling process, which can be described with the following equations:

Birth $X \xrightarrow{\lambda} 2X$

Death $X \xrightarrow{\mu} \emptyset$

Sampling $X \xrightarrow{\psi} \text{Sequence}$

This process continues until one of three conditions are met: the stopping time, T_{stop} is reached, the prevalence of infection reaches 50,000, or there are 1,000 sequenced infections. The realizations of this process are conditioned to have at least two sequenced infections and for the pathogen not to have gone extinct before the end of the process.

8. Compute the reconstructed tree by tracking transmission among the individuals in the birth-death-sampling process and who was sampled. We can reconstruct a transmission tree (Fig. 1A) describing who-infected-whom and the circumstances under which they ceased to be infectious (i.e. whether they were sampled when they ceased to be infectious). This can then be pruned to obtain a reconstructed tree connecting the sequenced infections (Fig. 1B).
9. Generate a collection of *measurements* of the simulation. Each measurement is a vector

$$M_i = (t_m, N_p(t_m), N_c(t_m), \mathcal{R}(t_m))$$

where we have sampled the measurement time randomly $t_m \sim U(0, t_{\text{present}})$ (see Fig. 1.)

10. Record the set of measurements, $\{M_i^{(j)}\}$ and the corresponding reconstructed tree, $\mathcal{T}^{(j)}$, from this j th realization of the process. By repeating this N_{train} many times, we generate our training dataset: $\mathcal{D}_{\text{train}} = \{(\mathcal{T}_j, \{M_i^{(j)}\})\}$.

Quantity	Prior	Median (95% interval)
Model parameters		
Reproduction number	lognormal (1.0, 0.7)	2.72 (0.69, 10.72)
Net removal rate	lognormal (-1.81, 0.2)	0.16 (0.11, 0.24)
Sampled proportion	Beta (1.1, 8.0)	0.094 (0.005, 0.384)
Hyperparameters		
Epidemic duration (in days)	Discrete-uniform{30, ..., 90}	
Number of parameter changes	Discrete-uniform{1, 2}	
Change times	U (0, T_{stop})	

Table 4: The prior distribution used in the simulations along with summary statistics to indicate typical samples.

7.2 Sensitivity analysis

7.2.1 Alternative model with delayed sampling

As a sensitivity analysis, we consider an alternative simulation model in which there is *delayed sampling*: there is an initial interval during which the sampling rate is set to zero, after which sampling is activated and remains constant. The sampled proportion (i.e., the sampling intensity once activated) is drawn from the same marginal distribution used to generate the sampling proportions for the original training dataset.

The activation time of the sampling is chosen uniformly as a proportion of the full epidemic duration, with the proportion drawn from $t_{\text{act}} \sim \text{U}(0.3, 0.7)$. Consequently, this alternative model generates datasets in which there is a period of unobserved transmission early in the epidemic, during which infections accumulate but no sequences are observed.

All other aspects of the simulation model are defined as in the original simulation: the reproduction number, \mathcal{R} , is specified in the same way (piece-wise constant between change times, with values drawn from the prior), and the net removal rate is once again constant with $\sigma \sim \text{lognormal}(-1.81, 0.2)$. The key difference is that the sampling proportion is a piece-wise function with a single change point: before the activation time, $t < t_{\text{act}}T_{\text{stop}}$, the sampling proportion is $p_{\psi}(t) = 0$, and after activation, $t \geq t_{\text{act}}T_{\text{stop}}$, it is constant, $p_{\psi}(t) = p_{\psi}^i$, with $p_{\psi}^i \sim \text{Beta}(1.1, 8.0)$.

7.2.2 Sensitivity to choice of prior distribution

A further simulation study was carried out to assess the impact of misspecifying the prior distribution. We considered two potential prior distributions: a *basic* distribution, and a more diffuse *noisy* distribution. In Fig. SI5 we show the basic and noisy prior distributions for \mathcal{R} and the epidemic duration, T_{stop} . Prior distributions for all other parameters are the same between the two cases. We considered four variations of the NBE in this sensitivity analysis:

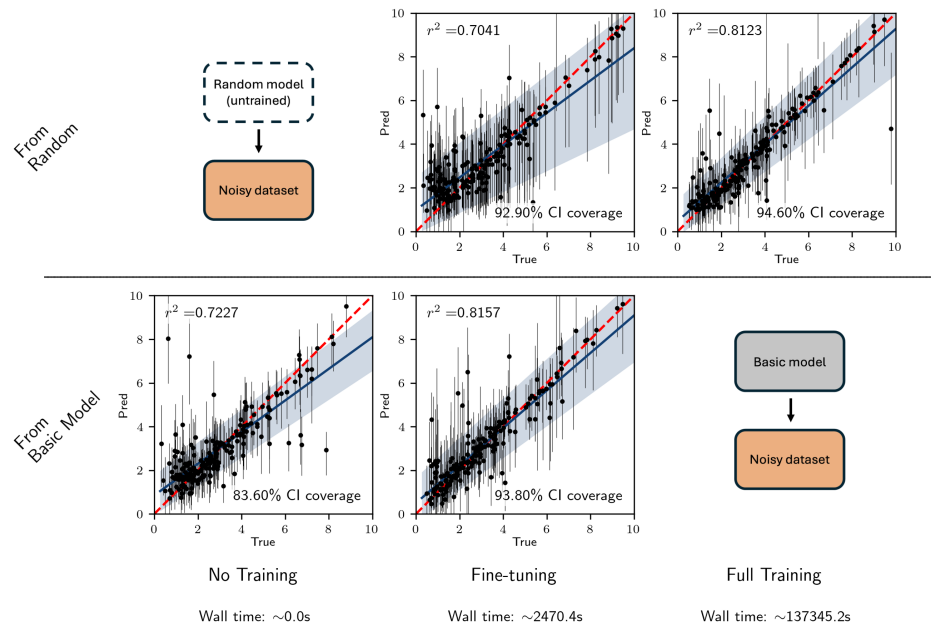
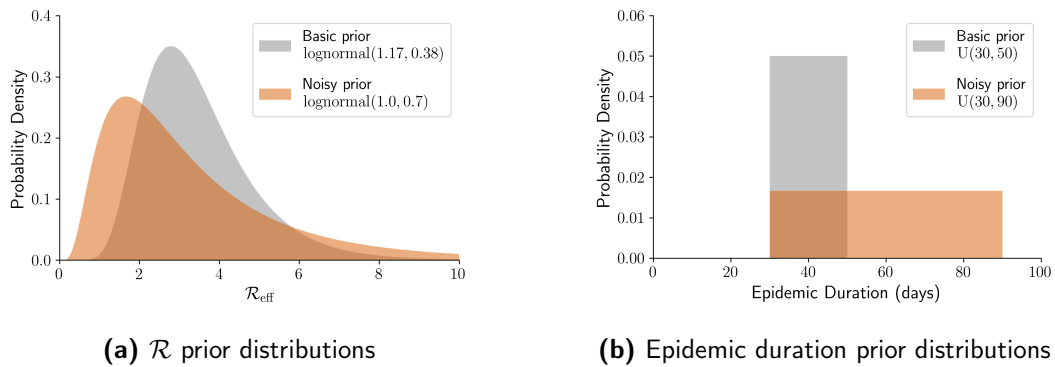
Zero-shot pre-trained a model trained on the basic distribution which is then applied to data drawn from the noisy distribution;

Fine-tuned pre-trained a model trained on the basic distribution and subsequently fine-tuned on data from the noisy distribution is then applied to data from the noisy distribution;

Fine-tuned from random a model in which the weights are randomly initialized, and only the weights of f_{pred} are modified during training is then applied to data simulated from the noisy distribution; and

Full training from random a model in which the weights are randomly initialized and the model is trained on data simulated from the noisy distribution, which is then applied to data simulated from the noisy distribution.

In Tab. SI5 we present the time taken to pre-train or fine-tune each model variant and the resulting performance as measured by the coefficient of determination, R^2 , for the estimates of $\mathcal{R}(t)$, $\log_{10}(N_p(t))$, and $\log_{10}(N_c(t))$. This demonstrates that fine-tuning an existing model takes orders of magnitude less time than training a model from scratch and results in comparable performance.



(c) Estimates from model variants

Figure 5: NBEs can be rapidly retrained to adapt to different prior distributions. (a) and (b) show the basic and noisy distributions considered. (c) shows the true values and the estimates of the basic reproduction number sampled from the noisy prior. The models used to generate the estimates start from either a random initialization (top row) or a model pre-trained on data sampled from the basic prior. We show the performance for three levels of training: no training (for the basic model), fine-tuning (for both models), and full training (from the random model). For each level of training we also show the indicative wall time required.

Training	Wall time (seconds)	\mathcal{R} (R^2)	$\log_{10}(N_p)$ (R^2)	$\log_{10}(N_c)$ (R^2)
Zero-shot pre-trained	0.0	0.723	0.924	0.933
Fine-tuned pre-trained	<u>2315.6</u>	0.816	<u>0.944</u>	<u>0.952</u>
Fine-tuned from random	2470.4	0.704	0.817	0.860
Full training from random	137345.2	<u>0.812</u>	0.955	0.962

Table 5: The NBE performs reasonably well when applied to test data drawn from a more diffuse prior (as depicted in Fig. S15). For each model, this shows the training time and the coefficient of determination, R^2 for each of the quantities of interest: \mathcal{R} , the reproduction number; $\log_{10}(N_p)$, the common logarithm of the prevalence; and $\log_{10}(N_c)$, the common logarithm of the cumulative incidence. With a small amount of fine-tuning of the neural network, the estimators performance matches that of a model trained from scratch, suggesting a way forward for re-use of NBEs.

7.3 BEAST2 MCMC using BDSky

For the MCMC baseline, we used the Birth-Death Skyline (BDSky) tree prior (Stadler et al., 2013) implemented in BEAST2 (Bouckaert et al., 2019). To align this analysis with the simulation study and isolate inference of epidemiological parameters, we fixed the phylogeny to the true reconstructed tree and fixed the becoming-uninfectious rate at its true value. The MCMC therefore estimated only two quantities: the effective reproduction number and the sampling proportion. The effective reproduction number was parameterized as a piece-wise constant trajectory with 10 values uniformly spaced through time, while the sampling proportion was modeled as a single constant parameter over time.

For each of the testing datasets, we ran one chain for 5,000,000 iterations and retained 5,000 posterior samples via thinning. For all runs, effective sample sizes were greater than 200. Priors for the values of both the reproduction number and the sampling proportion matched those used when generating the testing data (Tab. SI4).